Molecular Fluorescent Probes for Imaging and Evaluation of Hypochlorite Fluctuations during Diagnosis and Therapy of Osteoarthritis in Cells and in a Mouse Model

Ji-Ting Hou,[§] Bingya Wang,[§] Yuxia Zou,[§] Peiwen Fan, Xueping Chang, Xinhua Cao,* Shan Wang,* and Fabiao Yu*

Read Online

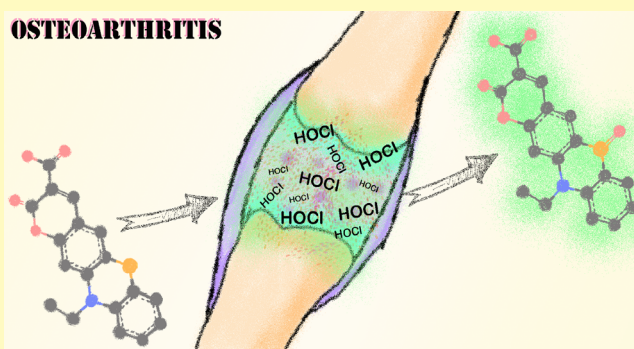ACCESS | Metrics & More | Article Recommendations | Supporting Information

ABSTRACT: The early diagnosis of osteoarthritis (OA) can halt or delay the progression of the disease, and it is essentially beneficial to its treatment. However, biomarkers with sufficient sensitivity for dynamically identifying early OA are still yet to be determined. The overproduced hypochlorous acid (HOCl) has been proposed as an obvious symptom in early OA. Herein, based on the oxidation reaction of the sulfur atom in phenothiazine into sulfoxide, we design and synthesize a phenothiazine-derived coumarin fluorescent probe **PDC** for the detection of ClO⁻ in cells and in an OA mouse model. The probe **PDC** exhibits excellent selectivity and sensitivity for ClO⁻ detection with a limit of detection as low as 16.1 nM. Taking advantage of the probe **PDC**, we visualize and evaluate the level changes of ClO⁻ in macrophage cells, which is stimulated by various inflammatory factors. The anti-inflammatory and therapeutic effects of selenocysteine and methotrexate in inflamed cells are also confirmed. Finally, with in vivo imaging of ClO⁻ concentration changes in OA BALB/c mouse models, we successfully inspected the relationship between OA phenotypes and the burst of ClO⁻. We suggest that abnormal changes in HOCl concentration may be considered as a new biomarker for the early OA diagnosis.

KEYWORDS: fluorescent probe, hypochlorite, osteoarthritis, inflammation, mouse model

INTRODUCTION

Osteoarthritis (OA) is a chronic and degenerative joint disorder in which articular cartilage injury and reactive hyperplasia of the joint edge and subchondral bone are involved owing to various risk factors, including aging, obesity, strain, trauma, and joint congenital abnormalities.[1,2] The structural abnormalities in joints are often accompanied by pain and joint dysfunctions, which severely impair the living quality of patients. However, OA is quite challenging to cure. As is well known, in the early stages of OA, articular cartilage is more metabolically adapted to its new environment, and the cartilage matrix is more easily repaired and regenerated than that at advanced stages of OA.[3,4] Therefore, the early diagnosis of OA have priority to hinder or prevent the progression of the disease, and it may be beneficial to the treatment. Magnetic resonance imaging (MRI) has been regarded as the most widely used imaging technique for clinical diagnosis of OA. Nevertheless, many structural abnormalities detected by MRI are very common in older populations, which may cause the diagnostic uncertainty for OA patients, and are not suitable for early diagnosis of OA.[5] Therefore, it is invaluable to exploit

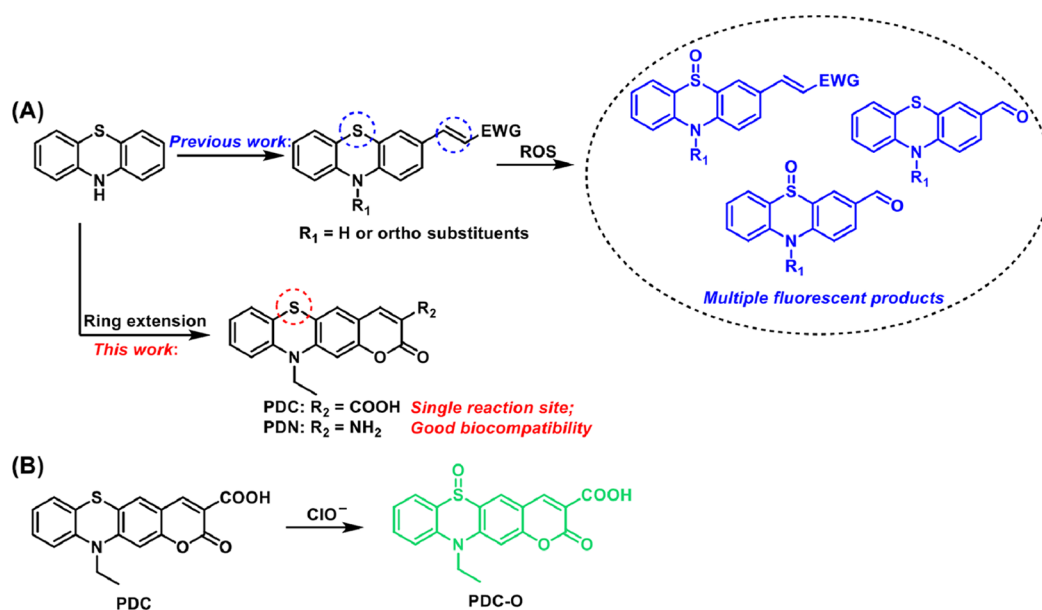new biomarkers with sufficient sensitivity for identifying early OA.

It is now suggested that a low-grade inflammation is implicated in OA,[6,7] which induces the accumulation of neutrophils and macrophages in impaired joints. Then, myeloperoxidase (MPO), a specific enzyme, is overproduced in these cells. In patients with early OA, a 4-fold increase in MPO levels has been found in comparison with patients without OA or with advanced OA.[8] Accordingly, hypochlorous acid (HOCl, in this work mainly as ClO⁻), a type of reactive oxygen species (ROS, generally including ·OH, $O_2^{·-}$, ONOO⁻, $^1O_2$, ClO⁻, and H_2O_2), is over-generated in early OA through an MPO-catalyzed reaction between H_2O_2 and Cl⁻.[9] It is proposed that HOCl is involved in the degradative process of articular cartilage in early OA based on an indirect detection of

Scheme 1. (A) Design Strategy of Phenothiazine-Derived Fluorescent Probes; (B) Proposed Reaction Mechanism between Probe PDC and ClO

its chlorinated products via in vitro analysis like HPLC−MS.[8,10] However, such methods are not suitable for in situ measurement and cannot provide reliable information on the real-time fluctuation of ClO⁻ levels in early OA and thus cannot reflect the dynamic progression of the disease. As such, compared with its secondary products, ClO⁻ must present a more ideal biomarker candidate for the determination of early OA owing to their direct association. Combined with traditional detection methods like MRI, early OA may be diagnosed with the observation of ClO⁻ generation in the joint of patients. Thus, it is urgent to develop a sensitive and selective chemical tool for the direct visualization and evaluation of ClO⁻ changes during the development of OA.

Due to their ability for in situ detection, rapid response, and noninvasive measurement,[11−16] a number of fluorescent probes have been constructed for sensing ClO⁻ over the past decades.[17−30] Although several probes have been utilized to image the generation of ClO⁻ in a commom arthritis model,[31−35] to the best of our knowledge, there is no certain fluorescent probe conceived to evaluate ClO⁻ in OA. Aware of this requirement, in this work, we prepared two phenothiazine-derived coumarin fluorescent probes **PDC** and **PDN** for the imaging and evaluation of ClO⁻ fluctuations in the early diagnosis of OA (Scheme 1). Encouragingly, the probe **PDC** exhibited a more highly selective and sensitive response toward ClO⁻ with a "turn-on" behavior, and it could be utilized to image endogenous ClO⁻ in RAW 264.7 macrophages that were treated with various inflammatory factors. Moreover, the remediation of injuried RAW 264.7 cells was achieved using antioxidants. Ultimately, the overproduction of ClO⁻ in OA mouse models induced by lipopolysaccharide (LPS) was successfully visualized for the first time, as well as its remediation via the administration of selenocystine (Sec). By making use of ClO⁻ as a potential biomarker, it was promising that the probe **PDC** could be considered as a potent auxiliary chemical tool to indicate the early OA in patients.

■ EXPERIMENTAL SECTION

General Remarks for Experimental. All chemicals were purchased from Aladdin and Energy Chemical and were used without further purification. ^{1}H NMR and ^{13}C NMR spectra were measured on a 600 MHz NMR spectrometer. Proton chemical shifts of NMR spectra are given in ppm relative to internals reference TMS (^{1}H, 0.00 ppm). Mass spectra were measured on an HP-1100 LC−MS spectrometer. UV−vis spectra were recorded on a UV-3900 spectrometer. Fluorescence spectra were recorded on an FLS 1000 fluorimeter. Confocal microscopy fluorescence images were acquired on a Leica TCS SP8. The solvents used for UV−vis and fluorescence measurements were of HPLC grade. Unless otherwise noted, materials were obtained from commercial suppliers and were used without further purification. All the solvents were dried according to the standard methods prior to use. All of the solvents were either HPLC or spectroscopic grade in the optical spectroscopic studies.

Preparation and Characterization of 2. Compound **1** was prepared following a previous report.[36] Compound **1** (3.2 g, 11.8 mmol) was dissolved in 20 mL of EtOH, and then diethyl malonate (3.8 g, 23.6 mmol) was added in a portion. The reaction mixture was heated to 80 °C for reflux. After 8 h, the reaction was cooled down to room temperature, and the precipitate was filtered to afford **2** as a red solid (3.9 g, 90.6%).^{1}H NMR (600 MHz, DMSO-d_6) δ 8.53 (s, 1H), 7.57 (s, 1H), 7.22−7.17 (m, 1H), 7.13 (dd, J = 7.6, 1.5 Hz, 1H), 7.10−7.07 (m, 1H), 6.98 (td, J = 7.5, 1.1 Hz, 1H), 6.94 (s, 1H), 4.22 (q, J = 7.1 Hz, 2H), 3.98 (q, J = 6.9 Hz, 2H), 1.28 (t, J = 6.9 Hz, 3H), 1.25 (t, J = 7.1 Hz, 3H). ^{13}C NMR (150 MHz, DMSO-d_6) δ 163.36, 156.79, 156.78, 150.33, 148.57, 142.06, 128.62, 127.66, 127.37, 124.37, 121.96, 119.23, 116.97, 113.31, 113.20, 102.31, 61.44, 42.70, 14.67, 12.72.

Preparation and Characterization of PDC. Compound **2** (3 g, 8.2 mmol) was dissolved in EtOH (60 mL), and 10% NaOH (80 mL) was added. The mixture was refluxed for 30 min and then cooled down to room temperature. The reaction mixture was adjusted to pH 2−3 with con. HCl. The precipitate was filtered to afford **PDC** as a dark-red solid (2.6 g, 95%). ^{1}H NMR (600 MHz, DMSO-d_6) δ 8.53 (s, 1H), 7.58−7.53 (m, 1H), 7.19 (t, J = 7.8 Hz, 1H), 7.12 (d, J = 7.5 Hz, 1H), 7.07 (d, J = 8.1 Hz, 1H), 6.97 (t, J = 7.4 Hz, 1H), 6.93 (d, J = 3.3 Hz, 1H), 3.97 (q, J = 6.6 Hz, 2H), 1.28 (t, J = 6.9 Hz, 3H). ^{13}C NMR (150 MHz, DMSO-d_6) δ 164.62, 157.83, 156.67, 150.21, 148.43, 142.13, 128.60, 127.65, 127.30, 124.34, 122.03, 119.35, 116.95, 113.88, 113.39, 102.34, 42.69, 12.74. ESI-MS: m/z 340.0643 [M + H]$^+$: (calcd 340.0638).

Preparation and Characterization of 3. To a solution of compound **1** (542 mg, 2.0 mmol) and ethyl nitroacetate (293 mg, 2.2 mmol) in *n*-butanol (20 mL) were added piperidine (50 μL) and acetate acid (100 μL). The mixture was refluxed at 118 °C for 10 h and then cooled down to room temperature. The precipitate was filtered to afford **3** as a dark-red solid (380 mg, 55.9%). ^{1}H NMR (600 MHz, DMSO-d_6) δ 9.00 (s, 1H), 7.63 (s, 1H), 7.26−7.18 (m, 1H), 7.13 (td, J = 7.7, 1.3 Hz, 2H), 7.06−6.98 (m, 2H), 4.01 (q, J = 6.9 Hz, 2H), 1.29 (t, J = 6.9 Hz, 3H). ^{13}C NMR (150 MHz, DMSO-d_6) δ 157.29, 152.81, 151.74, 143.46, 141.28, 131.04, 128.77, 128.10, 127.68, 124.86, 121.61, 120.02, 117.28, 111.93, 102.12, 43.10, 12.66. ESI-MS: m/z 341.0573 [M + H]$^+$: (calcd 341.0591).

Preparation and Characterization of PDN. Hydrochloric acid (5 mL, 15%) was slowly added to a solution of compound **3** (340 mg, 1 mmol) and SnCl$_2$·2H$_2$O (564 mg, 2.5 mmol) in ethyl acetate (EA, 25 mL). The reaction mixture was refluxed for 8 h. After the solvent was evaporated, the residue was neutralized with 15% NaOH to pH 5−6 and extracted with EA. The combined organic phase was washed with brine and dried over Na$_2$SO$_4$. The crude product was purified over silica gel by column chromatography using a mixture of petroleum ether/EA (6:1, v/v) as the eluent to afford **PDN** as a yellow solid. (200 mg, 64.5%). ^{1}H NMR (600 MHz, chloroform-d) δ 7.16 (ddd, J = 8.7, 7.8, 1.6 Hz, 1H), 7.11 (dd, J = 7.6, 1.5 Hz, 1H), 6.98 (s, 1H), 6.93 (td, J = 7.5, 1.5 Hz, 1H), 6.90−6.87 (m, 1H), 6.75 (s, 1H), 6.59 (s, 1H), 3.91 (q, J = 7.0 Hz, 2H), 1.43 (t, J = 6.9 Hz, 3H). ^{13}C NMR (150 MHz, chloroform-d) δ 159.64, 149.40, 144.12, 143.96, 130.08, 127.61, 127.43, 123.47, 122.86, 122.42, 121.01, 115.90, 115.44, 111.32, 102.82, 42.35, 12.77. ESI-MS: m/z 333.0658 [M + Na]$^+$: (calcd 333.0668).

Preparation and Characterization of PDC-O. To 300 mL of water was added a solution of **PDC** (14.0 mg, 41.3 μmol) in 1 mL of DMSO. Under stirring using a 365 nm UV lamp, aqueous NaClO (available chlorine 5.5 ∼ 6.5%) was added to the mixture dropwise until the fluorescence color changed into cyan completely. Then, con. HCl was added to adjust the pH of the solution to ∼5. The reaction mixture was extracted with CH$_2$Cl$_2$ (3× 30 mL). The combined organic phase was washed with brine and dried over Na$_2$SO$_4$. The final removal of the solvent afforded **PDC-O** as a yellow solid. (14.1 mg, 95.9%). ^{1}H NMR (600 MHz, DMSO-d_6) δ 8.82 (s, 1H), 8.64 (s, 1H), 8.05 (d, J = 6.7 Hz, 1H), 7.80−7.78 (d, J = 3.1 Hz, 2H), 7.62 (s, 1H), 7.43−7.37 (m, 1H), 4.48 (q, J = 7.0 Hz, 2H), 1.45 (t, J = 6.9 Hz, 3H). ^{13}C NMR (150 MHz, DMSO-d_6) δ 163.91, 157.29, 156.52, 147.77, 141.43, 136.61, 134.74, 133.59, 131.54, 124.39, 123.07, 121.61, 116.90, 115.39, 112.60, 102.28, 42.64, 11.53. ESI-MS: m/z 356.0573 [M + H]$^+$: (calcd 356.0587).

Cell Counting Kit-8 Assay for Probes. RAW 264.7 cells were cultured in DMEM supplemented with 10% FBS in an atmosphere of 5% CO$_2$ and 95% air at 37 °C. The cells (8000 cell/well) were plated into 96-well plates and allowed to adhere for 24 h. Subsequently, the cells were incubated with 0.001, 10, 20, 30, 40, 50, 60, 70, 80, 90, and 100 μM (final concentration) of the probe at 37 °C in an atmosphere of 5% CO$_2$ and 95% air for 24 h. An untreated assay with DMEM was also performed under the same conditions as those in the control. CCK-8 solution (5.0 mg/mL, 10 μL) was added to each well. Then, the plate was incubated in an atmosphere of 5% CO$_2$ and 95% air. One hour later, the absorbance was measured at 450 nm using a microplate reader (TECAN infinite M200pro).

Cell Culture and Confocal Imaging. For imaging experiments, a probe with a purity of above 95% was used. RAW 264.7 cells were incubated in DMEM supplemented with 10% fetal bovine serum (FBS). The cultures were maintained at 37 °C in an atmosphere of 95% air with 5% CO$_2$. Living cells were first inoculated to a confocal plate followed by adding 1 mL of fresh complete culture media and cultured for 24 h. Then, the cells were incubated with 10 μM probe solution for 10 min. After that, probe **PDC**-loaded cells were incubated with various stimuli for 30, 60, and 90 min before imaging experiments. Confocal images of cells were obtained using an Olympus FV3000 confocal microscope with a 60× oil objective lens. The excitation wavelength selected was 405 nm, and the collected wavelengths selected were 480−510 nm.

In Vivo Imaging in Living Mice Models. Six to eight week-old BALB/c mice were provided by Hainan Medical University. The right knees of the six to eight week-old BALB/c mice were injected with LPS (0.1 mL, 5 mg/mL, PBS, intra-articular injection) every day; the probe **PDC** (0.1 mL, 10 μM, DMSO/PBS = 1:1, V:V, intra-articular injection) before in vivo imaging after a few weeks; (Sec)$_2$ (500 μg/ kg) was i.p. injected every day before LPS administration; MTX (100 μg/kg) was i.p. injected every day before LPS administration. The hair around the knee was removed during the research. Images were taken using a PerkinElmer IVIS Lumina XRMS Series III in vivo imaging system, with an excitation filter of 405 nm and emission windows from 480 to 510 nm. All experimental procedures were conducted in conformity with institutional guidelines for the care and use of laboratory animals, and protocols were approved by the Institutional Animal Care and Use Committee in Hainan Medical University, Haikou, China.
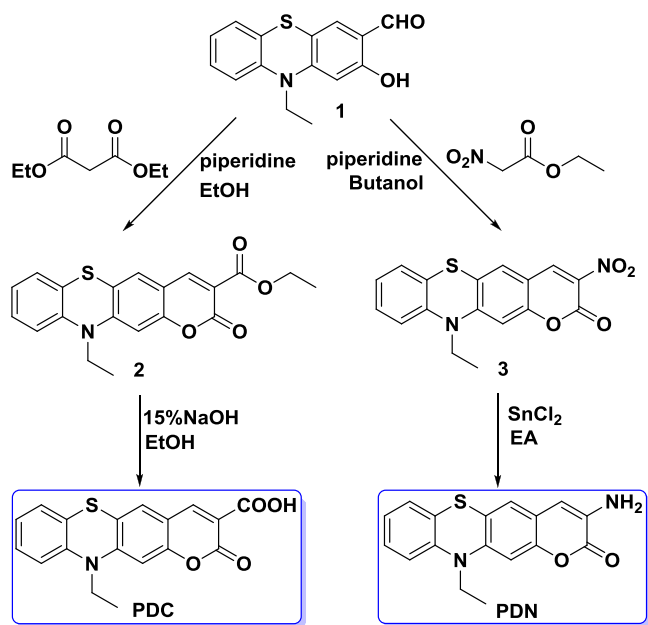
■ RESULTS AND DISCUSSION

Design Strategy and Synthesis of the Probes PDC and PDN. Over the past several years, phenothiazine has been employed as a block unit for the design of ClO$^-$-specific fluorescent probes due to its oxidizable sulfur atom.[37−39] As illustrated in Scheme 1A, in those probes, electron-withdrawing groups (EWGs) have usually been incorporated at the 3-position of the phenothiazine backbone to construct large π conjugations with intramolecular charge transfer (ICT), while their optical behaviors are obviously altered upon the oxidation of the sulfur atom to sulfoxide by ClO$^-$. However, besides the oxidizable sulfur atom, the introduced C=C bond is always susceptible to ROS, increasing the uncertainty of the reaction between the probes and ROS. In addition, these dual reaction sites often lead to the generation of multiple fluorescent products that may affect the accuracy of measurements.[40] Moreover, the additional reactive site may weaken the probes' selectivity to ClO$^-$. On the other hand, coumarin widely exists in natural products and has been vastly utilized in the creation of fluorescent probes because of its splendid photophysical properties.[41] Thus, a new strategy to construct phenothiazine-derived coumarin analogues for fluorescent detection of ClO$^-$ is presented in this work by ring extension that amplifies the π systems but avoids the introduction of additional reactive sites. Such derivatives may be highly biocompatible with good optical properties and has a single reaction site at the sulfur atom. As indicated in Scheme 1, the probes **PDC** and **PDN** comprised carboxyl and amino groups on the coumarin ring, respectively, which resulted in their different response toward ROS. We hypothesized the reason could be attributed to distinct electronic effect of the respective substituents (Figure 2, density functional theory (DFT) calculations).

The two probes **PDC** and **PDN** were synthesized from the phenothiazine intermediate **3** with a salicylaldehyde structure (Scheme 2). Knoevenagel condensation between **3** and diethyl malonate gave the phenothiazine-fused coumarin derivative **4**, which further underwent saponification to afford probe **PDC** in a yield of 95%. In contrast, Knoevenagel condensation between **3** and ethyl nitroacetate yielded nitrifying intermediate **5**. Final reduction of **5** with stannous chloride gave probe **PDN** in a yield of 64.5%.

Reaction Mechanism and Selectivity of Probes PDC and PDN toward ClO$^-$. Initially, the optical responses of probes **PDC** and **PDN** toward ROS were investigated. In PBS buffer (pH 7.2−7.4, 10 mM), a main absorption band centered at 415 nm (ε = 15,300 M^{-1} cm^{-1}) was found in the UV−vis absorption spectrum of probe **PDC** (Figure S1). Upon

Scheme 2. Synthesis of Probes

addition of 10 equiv of ClO⁻, the absorbance at 415 nm disappeared, along with the appearance of a new peak centered at 377 nm and a color change from yellow to colorless, indicating a complete reaction between probe **PDC** and ClO⁻.

The reaction product was confirmed using HRMS analysis. An apparent ion peak at m/z 356.0605 was observed in the MS spectrum of the reaction mixture (Figure S2), which corresponded to the oxidative product **PDC-O** ([**PDC-O** + H]⁺: calcd 356.0587) (Scheme 1B). Further, we performed a constant reaction between **PDC** and NaClO and isolated the product **PDC-O**. The ¹H NMR spectra of **PDC** and **PDC-O** in DMSO-d_6 were then compared. As seen in Figure S3, all proton signals in **PDC-O** was down-shifted in comparison to those in **PDC**, which was ascribed to the formation of an electron-withdrawing sulfoxide moiety. It is noteworthy that in the reaction, **PDC-O** was obtained in a high yield of ~96%, implying the nearly complete conversion of **PDC** into **PDC-O** by ClO⁻. This result affirmed our design strategy to increase the conversion efficiency of phenothiazine-based probes for ClO⁻. Thus, the response of probe **PDC** toward ClO⁻ was verified to be the oxidation of the sulfur atom in the phenothiazine unit into sulfoxide.[37−39]

When other ROS, including ˙OH, O₂˙⁻, ONOO⁻, H₂O₂, and ^{t}BuOOH, were added to the solution of probe **PDC**, the absorbance at 415 nm rarely showed changes, suggesting its high specificity toward ClO⁻. The results were also verified via fluorescence tests (Figure 1A). Probe **PDC** emitted faint fluorescence at 650 nm (quantum yield Φ = 0.89%) due to the strong ICT from the electron-rich phenothiazine unit to the electron-deficient carboxyl coumarin. Upon oxidation by ClO⁻, the ICT process was blocked. A 540-fold emission enhancement at 503 nm (Φ = 7.8%) was subsequently observed (Figure 1B). A large Stokes shift of 126 nm for the oxidized product **PDC-O** was measured, which was extremely superior for bioimaging owing to avoidance of the scattered light. In contrast, the addition of other ROS caused negligible variations of the emission spectra of probe **PDC**, affirming the high selectivity of probe **PDC** toward ClO⁻. Considering that a carboxyl unit could complex with many metal ions, we also

measured the emission spectra of the probe toward common metal ions, including Ca²⁺, Zn²⁺, Cu²⁺, Hg²⁺, Ag⁺, and Pb²⁺. The results revealed that no fluorescence variations toward these metal ions were produced, reconfirming the high specifity of the probe (Figure S4).

When the carboxyl group in probe **PDC** was replaced by an amino moiety to give probe **PDN**, there appeared a distinct optical response toward ROS. In PBS solution (pH 7.2−7.4, 10 mM), probe **PDN** exhibited moderate emission at 539 nm because of its weaker ICT in comparison to that of probe **PDC**. Upon the addition of various ROS, dramatic fluorescence quenching was found in the cases of ClO⁻ and ONOO⁻, while no new emission peaks were generated (Figure S5), implying that probe **PDN** showed much poorer selectivity to ROS than probe **PDC**. Thus, **PDC** was chosen as the better candidate for ClO⁻ sensing.

Density Functional Theory (DFT) Calculations. To further interpret the reactivity difference between the probes **PDC** and **PDN**, we performed DFT calculations using Becke's three-parameter hybrid exchange functional and the Lee-Yang-Parr correlation functional (B3LYP) with the 6-311++G** basis set.[42,43] All DFT calculations were carried out using Gaussian 09.[44] As illustrated in Figure 2, the π electrons on the highest occupied molecular orbital (HOMO) of the probe **PDC** were primarily located on the whole heterocyclic ring, and the carboxyl moiety essentially contributed little to its HOMO. By contrast, the amino group in probe PDN provided a large contribution to its HOMO. The big difference in the electron contribution of carboxyl and amino units might lead to the difference in the electron cloud density at the sulfur atom in both probes. In the optimized structures of probes **PDC** and **PDN**, the Mulliken charges of sulfur atoms were calculated to be 0.197 and 0.173 (Figure S6), respectively, indicating that the sulfur atom in probe **PDN** was more electron-rich, thus accounting for its higher susceptibility toward ROS. Hence, an electron-withdrawing group on the coumarin ring was supposed to decrease the electron density at the sulfur atom, which could improve its response selectivity toward ROS. Furthermore, by the merits of time-dependent DFT (TD-DFT) calculations, the oscillator strengths f of probe **PDC** and its oxidized product **PDC-O** were determined to be 0.2600 and 0.5625, respectively, which was consistent with the emission enhancement of probe **PDC** upon reaction with ClO⁻.

Spectral Properties of Probe PDC toward ClO⁻. Having demonstrated its excellent selectivity toward ClO⁻, we next examined the spectral behaviors of probe **PDC** with ClO⁻ in detail. First, titration tests were conducted. When increasing doses of ClO⁻ were added to the solution of probe **PDC**, the absorption band at 415 nm decreased gradually, accompanied by the generation of a new peak at 377 nm (Figure 1C). An isosbestic point at 400 nm was detected, signifying the generation of a single absorptive product in the reaction. The blue shift from 415 to 377 nm was attributed to the blocked ICT process resulting from the oxidiation of the sulfur atom. Meanwhile, the fluorescence intensity of probe **PDC** at 503 nm was synchronously reinforced and kept steady when 10 equiv of ClO⁻ was added (Figure 1D,E). A linear relationship between the fluorescence intensity at 503 nm (I_{503}) and the concentrations of ClO⁻ in the range of 0−5 μM was calibrated (Figure 1F). According to the titration profile, the limit of detection toward ClO⁻ was determined to be 16.1
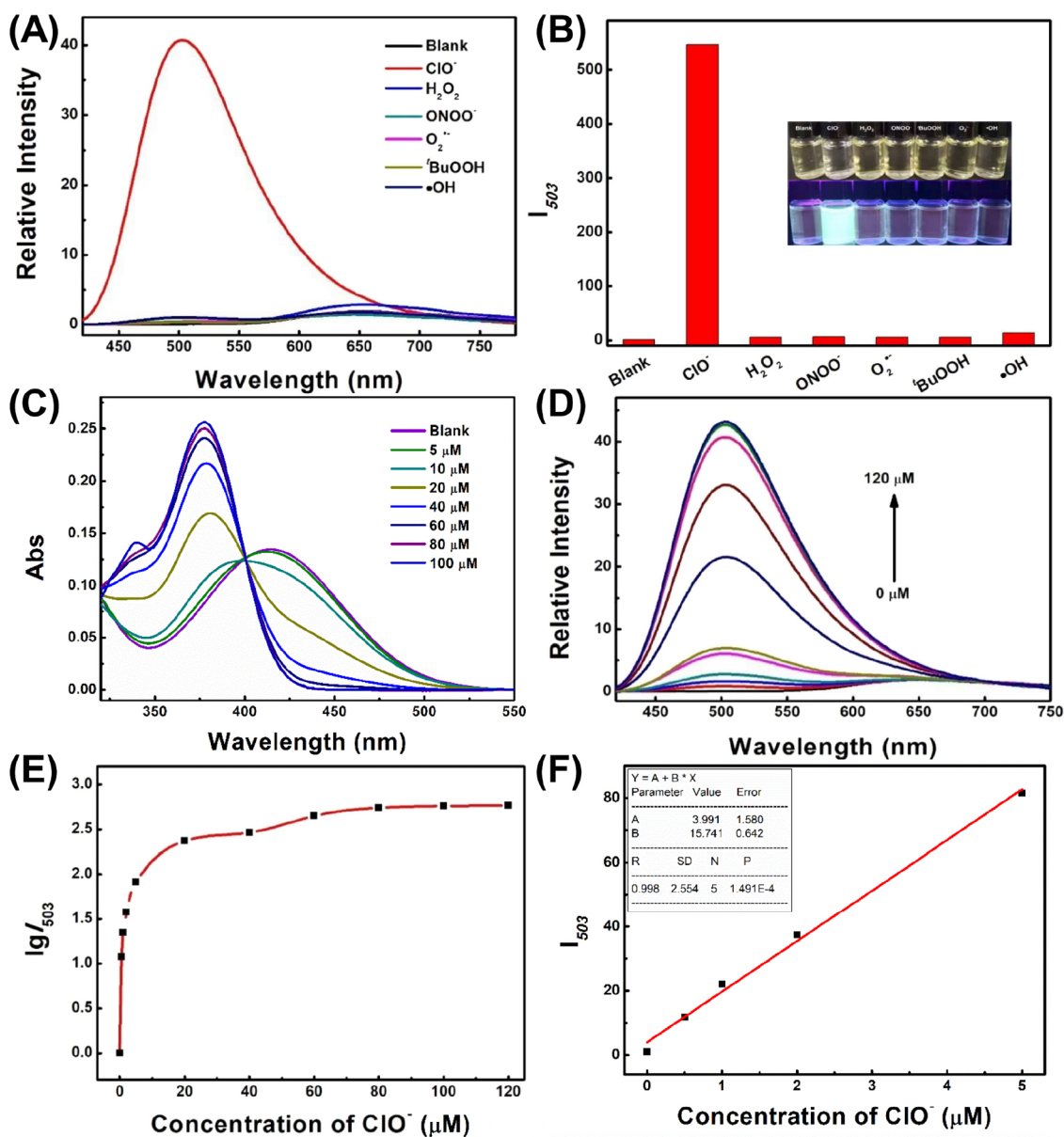
Figure 1. (A) Emission spectra of the probe **PDC** (10 μM) before and after addition of various reactive species (100 μM) in PBS solution (pH 7.2−7.4, 10 mM); (B) intensity changes of **PDC** before and after addition of various reactive species. Inset: photography of probe **PDC** with or without ROS under daylight (top) and a 365 nm UV lamp (bottom), respectively; (C) UV−vis titration of **PDC** toward various concentrations of ClO$^-$ in PBS solution.; (D) fluorescence titration of **PDC** (10 μM) toward various concentrations of ClO$^-$ in PBS solution; (E) relationship between lgI_{503} and ClO$^-$; (F) linear relationship between fluorescence intensity (I_{503}) of **PDC** (10 μM) and various concentrations of ClO$^-$. λ_{ex} = 400 nm; slit widths: 5 nm/5 nm.

nM, which is comparable to those of reported probes (Figure S7).[17−35]

The reaction kinetics between probe **PDC** and ClO$^-$ was verified using time-dependent fluorescence measurement. The fluorescence intensity of probe **PDC** at 503 nm was very weak in the initial 100 s of reaction, while a sharp increase was observed within seconds after ClO$^-$ was added, confirming the real-time detection of ClO$^-$ with probe **PDC** (Figure S8). Photostability is another feature necessary for bioimaging. Upon continuous irradiation with a xenon lamp at 400 nm for 1 h, the emission intensity of **PDC** and **PDC-O** at 503 nm remained virtually unchanged, suggesting their superb resistance to photooxidation or photobleaching (Figure S9). Afterward, the fluorescence responses of probe **PDC** toward ClO$^-$ were examined in different buffered solutions with varied

pH values. In the pH range of 3.00−10.00, the emission intensity of probe **PDC** at 503 nm altered slightly, indicating its good pH tolerance. However, in the presence of ClO$^-$, an ∼100-fold enhancement was observed at pH 4.00. The intensity increased greatly with increased pH (Figure S10). These results suggested that although probe **PDC** showed a higher response to ClO$^-$ over HOCl, it could respond to HOCl/ClO$^-$ with sufficient sensitivity when the pH changed from 4.00 to 10.00, a range covering the whole physiological pH.

Evaluation of ClO$^-$ Level Changes in Cell Models. Inspired by its splendid optical properties, the detection of intracellular ClO$^-$ was carried out with probe **PDC**. The cytotoxicity of the probe in RAW 264.7 cells was first inspected using a CCK-8 assay. As shown in Figure S11, 90% of the cells
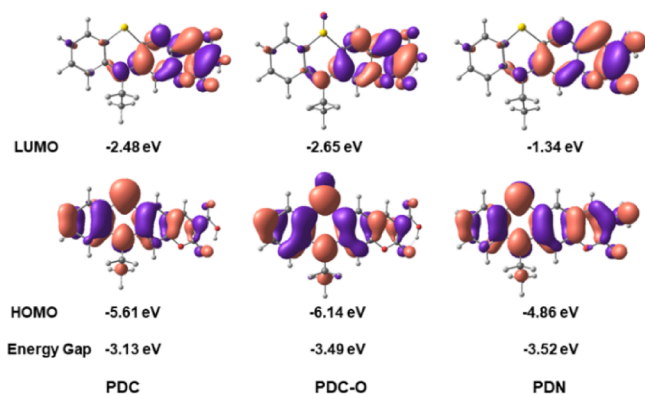
Figure 2. Molecular orbital plots for the lowest unoccupied molecular orbital (LUMO) and the highest occupied molecular orbital (HOMO) and the HOMO/LUMO energy gap of molecules **PDC**, **PDC-O**, and **PDN**.

were still alive when cultured with 50 μM probe for 24 h, and almost 80% of the cells survived even after incubation with 90 μM probe for 24 h. The median lethal dose LD$_{50}$ value of the probe was determined to be 257 μM in RAW 264.7 cells, demonstrating its low cytotoxicity and admirable biocompatibility.

Subsequently, the generation of ClO$^-$ in RAW 264.7 cells treated with different drugs was well evaluated using probe **PDC**. The stimulating factors including interleukin-1 (IL-1), tumor necrosis factor-α (TNF-α), and LPS were three types of stimuli that could induce inflammatory responses in cells. RAW 264.7 cells were treated with probe **PDC** for 10 min and then incubated with IL-1, TNF-α, or LPS for 0, 30, 60, and 90 min, respectively. As displayed in Figure 3, negligible fluorescence was visualized after 90 min in the control

group, indicating that our probe was stable in the complicated cellular micromilieu. Obvious fluorescence emission appeared when the probe-loaded cells were incubated with each stimulus for 30 min, suggesting that the probe was able to permeate the cell membrane and could sensitively image the generation of ClO$^-$ in stimulated cells. The fluroescence intensity from stimulated cells increased over time, consistent with the continous production of intracellular ClO$^-$ during inflammation. The ClO$^-$ burst after 90 min treatment represented by fluorescence signal intensity was ordered as follows: LPS > TNF-α > IL-1 (Figure S12). Furthermore, the strongest fluorescence was observed in cells treated with a combination of these three agents, suggesting that inflammation may be evoked by multiple factors. The fluorescence was mainly observed out of nucleus, (Figure S13), implying the localization of the probe molecules in the cytoplasm.

To further demonstrate the intracellular selectivity of **PDC** toward ClO$^-$, 4-aminobenzoic acid hydrazide (ABAH), a potent MPO inhibitor, was cultured with RAW 264.7 cells for 2 h before incubation with LPS for different time (0, 30, 60, and 90 min). As seen in Figure S14, the fluorescence intensity in ABAH-pre-treated cells was much lower than that in only LPS-treated cells, suggesting that the inhibition of MPO activity reduced the generation of ClO$^-$. Hence, the turn-on behavior of **PDC** in inflamed cells was essentially ascribed to the elevated MPO activity.

Sec has been recognized to play important roles in maintaining cellular redox balance[45] and has been demonstrated as a first-line antioxidant in cells against oxidative stress to protect cells and organisms from oxidative damage.[46] In an earlier work, we have inspected the protective effect of Sec in carbon disulfide-induced hepatitis.[47] On the other hand, methotrexate (MTX) is a standard drug for the treatment of rheumatoid arthritis (RA) by controlling synovial inflamma-
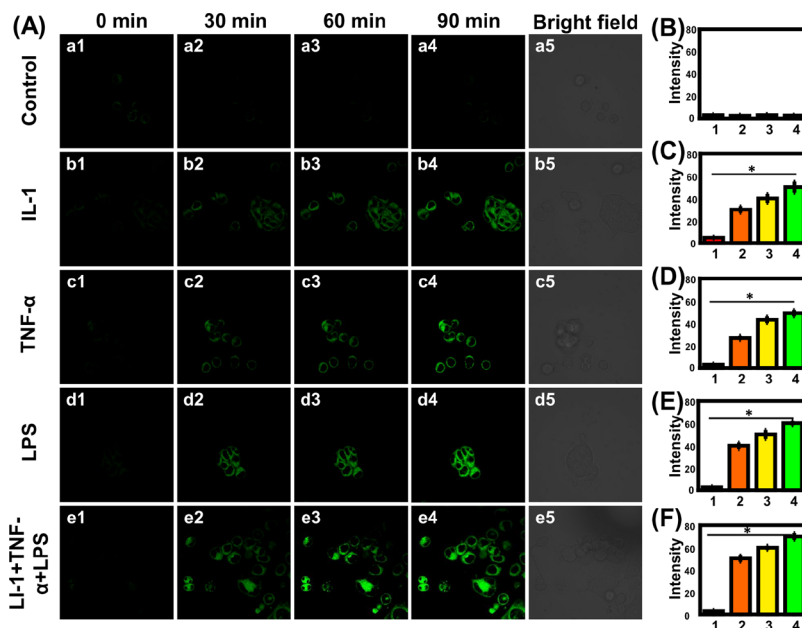

Figure 3. Evaluation of the generation of ClO$^-$ in RAW 264.7 cells treated with different stimuli using probe **PDC**. (A) Cells were treated with probe **PDC** for 10 min and then incubated with stimuli for 0, 30, 60, and 90 min before confocal imaging. (a) Control; (b) IL-1 (1.0 pg/mL); (c) TNF-α (1.0 pg./mL); (d) LPS (1.0 μg/mL); (e) IL-1&TNF-α&LPS (1.0 pg/mL, 1.0 pg/mL, and 1.0 μg/mL). (B) Fluorescence intensity collected from images a1−a4. (C) Fluorescence intensity collected from images b1−b4. (D) Fluorescence intensity collected from images c1−c4. (E) Fluorescence intensity collected from images d1−d4. (F) Fluorescence intensity collected from images e1−e4. Statistical analysis was performed using Student's t test ($n = 3$). *$P < 0.05$, error bars are mean ± SD, $n = 3$.
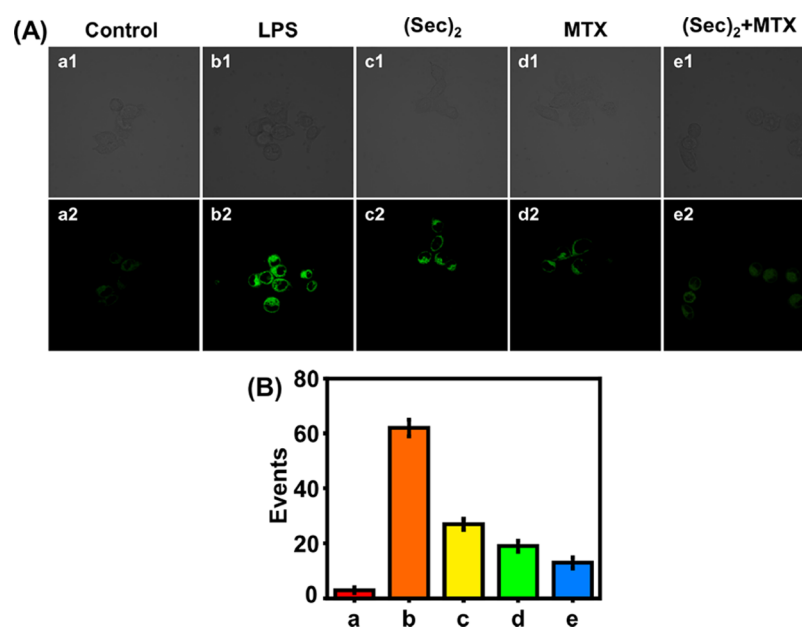
Figure 4. Protective effects of different agents in inflamed RAW 264.7 cells using probe **PDC**. (A) (a) Cells were treated with probe **PDC** for 10 min; (b) cells were incubated with LPS ($1.0 \ \mu g/mL$) for 36 h and then treated with probe **PDC** for 10 min; (c) cells were treated with LPS for 1 h and then co-cultured with (Sec)$_2$ ($1.0 \ \mu g/mL$) and LPS for another 35 h. Probe **PDC** was incubated for 10 min before imaging. (d) Cells were treated with LPS for 1 h and then cultured with MTX ($1.0 \ \mu g/mL$) for 35 h. Probe **PDC** was incubated for 10 min before imaging. (e) Cells were treated with LPS for 1 h and then cultured with (Sec)$_2$ ($1.0 \ \mu g/mL$) and MTX ($1.0 \ \mu g/mL$) for 35 h. Probe **PDC** was incubated for 10 min before imaging. (B) Fluorescence intensity collected from images a–e. Error bars are mean $\pm$ SD, $n = 3$.

tion, while it has been utilized for pain reduction in OA patients in recent studies.[48] Therefore, the anti-inflammatory effects of Sec and MTX were then evaluated in LPS-stimulated RAW 264.7 cells.

As shown in Figure 4A, the fluorescence in LPS-treated cells largely increased, while the co-incubation with selenocystine ((Sec)$_2$, the precursor to be converted into Sec in cells by dithiothreitol)[49] and MTX caused obvious emission intensity decrement, suggesting that the production of ClO$^-$ induced by LPS could be inhibited by Sec and MTX-triggered cytoprotective action. It should be noted here that the degree of fluorescence decline in the (Sec)$_2$ group was less than that in the MTX group, which implied that Sec displayed a weaker anti-inflammatory effect than MTX. However, the co-incubation of (Sec)$_2$ with MTX induced a maximum fluorescence reduction (Figure 4B). The results illustrated that the elimination of ClO$^-$ might be a key factor in MTX-triggered pain reduction in OA, and Sec could act as an auxiliary agent during MTX treatment.

In Vivo Imaging of ClO$^-$ in an OA Mouse Model. Encouraged by our results in in vitro tests, we carried out the in vivo imaging of ClO$^-$ generation in a BALB/c mouse model with OA phenotypes. The right knees of six to eight week-old BALB/c mice were injected with LPS every day, as this had been identified previously to contribute to the pathogenesis of OA.[50] As illustrated in Figure 5A, no detectable fluorescence was observed in mice injected with probes only, while an increasing fluorescence emission was visualized from the right knees with ongoing injection of LPS (Figure 5B), signifying the continuous accumulation of ClO$^-$ in the joint during the progression of OA. In the hematoxylin–eosin (H&E) images of tissue slices from LPS-treated joint (Figure 5G), macrophage infiltration (red arrows) and joint fluid (red arrows) were indicated in the articular cavity and the articular cartilage was severely damaged, confirming the initiation of OA.

Therefore, ClO$^-$ could be regarded as a new potential biomarker for the early diagnosis of OA with the aid of ClO$^-$-specific fluorescent probe **PDC**.

The protective effects of Sec and the treatment efficacy of MTX in OA mice were then investigated. As shown in Figure 5, the fluorescence intensity from OA mice pre-treated with (Sec)$_2$ or MTX showed a clear decrease compared to that in the LPS-group. The result demonstrated that the generation of ClO$^-$ was suppressed by both drugs. MTX exhibited a higher inhibitory effect than Sec did (Figure 5D,E). In the corresponding H&E images of joint slices from drug-treated groups (Figure 5G), fewer inflammatory cells were observed, and the articular cartilage was almost intactly present, illustrating the considerable protective effect of Sec and MTX in LPS-induced OA. The co-administration of (Sec)$_2$ with MTX exhibited the most powerful ClO$^-$ elimination and articular cartilage protection (Figure 5F). These combined results elucidated that LPS induced OA in mice and caused the accumulation of neutrophils and macrophages, thus resulting in the up-regulation of ClO$^-$. The ClO$^-$ level was positively related to the severity of OA. Moreover, Sec could be used as a protective antioxidant in combination with clinical drugs for the treatment of OA. Our experimental results indicated that ClO$^-$ could serve as a new potential biomarker for early OA diagnosis and its treatment.

■ CONCLUSIONS

In summary, we have developed two phenothiazine-derived coumarin probes **PDC** and **PDN** for the detection of ClO$^-$ in cells and in OA mouse models. Carboxyl-substituted probe **PDC** provides a higher sensitivity and selectivity toward ClO$^-$ in PBS compared with amino-substituted probe **PDN**. Probe **PDC** is also verified to be highly biocompatible and cell membrane-permeable. In RAW 264.7 cells stimulated by various inflammatory factors, the overgeneration of ClO$^-$ was
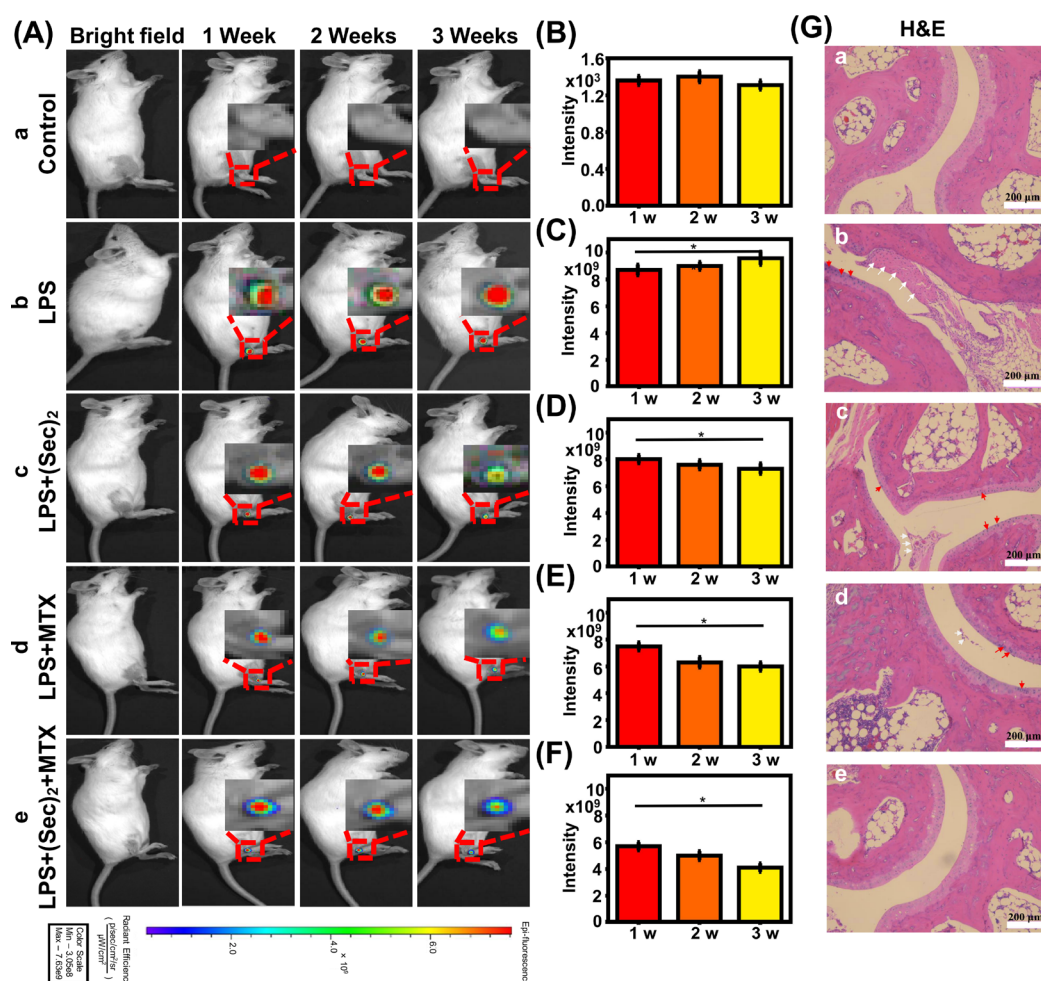
Figure 5. Protective effects of different agents in BALB/c mice with the OA model using probe **PDC**: (a) control. (b) right knees of six to eight week-old BALB/c mice injected with LPS (5 mg/mL, PBS) every day and then administered with probe **PDC** (0.1 mL, 10 μM, DMSO/PBS = 1:1, V:V) before in vivo imaging after a few weeks. (c) (Sec)2 (500 μg/kg) i.p. injected every day before LPS administration; (d) MTX (100 μg/kg) i.p. injected every day before LPS administration; (e) (Sec)2 (500 μg/kg) and MTX (100 μg/kg) i.p. injected every day before LPS administration. (B) Fluorescence intensity collected from (a); (C) fluorescence intensity collected from (b); (D) fluorescence intensity collected from image (c); (E) fluorescence intensity collected from image (d); (F) fluorescence intensity collected from image (e). Statistical analysis was performed using Student's t test ($n = 3$). *$P < 0.05$, error bars are $\pm$SD. (G) Representative H&E staining of the knee slices from the mice treated under various conditions.

further visualized using probe **PDC**, as well as the anti-inflammatory effects of Sec and MTX. Finally, in vivo imaging of ClO$^-$ in OA BALB/c mouse models was successfully performed for the first time. Based on the facts that low-grade inflammation is observed in OA and MPO is overexpressed in early OA, we speculated that HOCl was overproduced in early OA. Since our probe can sensitively detect HOCl upregulation in OA mice stimulated by LPS, it is a potential chemical tool for the diagnosis of early OA by using ClO$^-$ as a new potential biomarker.

ASSOCIATED CONTENT

Supporting Information

The Supporting Information is available free of charge at https://pubs.acs.org/doi/10.1021/acssensors.0c00270.

Additional experimental methods; NMR spectra; UV-vis absorption spectra of **PDC** before and after addition of various reactive species; ESI spectra of **PDC**; comparison of the ^{1}H NMR spectra between **PDC** and **PDC-O**; emission spectra of **PDC** and **PDN**; structures and the

Mulliken charge of the optimized probe **PDC** and probe **PDN**; linear relationship between fluorescence intensity and time-dependent fluorescence change of **PDC** and ClO$^-$; dynamic emission intensity of **PDC** with or without ClO$^-$; fluorescence emission intensity of **PDC** in the presence or absence of ClO$^-$; cytotoxicity of probe **PDC**; difference between fluorescence intensity from LPS, TNF-α or IL-1 groups; and probe-pre-treated Raw 264.7 cells incubated with LPS (PDF)

AUTHOR INFORMATION

Corresponding Authors

Xinhua Cao − *College of Chemistry and Chemical Engineering, Xinyang Normal University, Xinyang 464000, China;* Email: caoxh@xynu.edu.cn

Shan Wang − *College of Chemistry and Chemical Engineering, Xinyang Normal University, Xinyang 464000, China;* Email: smallcoral@live.cn

Fabiao Yu − *Key Laboratory of Emergency and Trauma, Ministry of Education, Key Laboratory of Hainan Trauma and*

Disaster Rescue, The First Affiliated Hospital of Hainan Medical University, Institute of Functional Materials and Molecular Imaging, Research Unit of Island Emergency Medicine, Chinese Academy of Medical Sciences (No. 2019RU013), College of Emergency and Trauma, Hainan Medical University, Haikou 571199, China; ⓘ orcid.org/ 0000-0003-0073-6299; Email: yufabiao@hainmc.edu.cn

Authors

Ji-Ting Hou — *College of Chemistry and Chemical Engineering, Xinyang Normal University, Xinyang 464000, China; Key Laboratory of Emergency and Trauma, Ministry of Education, Key Laboratory of Hainan Trauma and Disaster Rescue, The First Affiliated Hospital of Hainan Medical University, Institute of Functional Materials and Molecular Imaging, Research Unit of Island Emergency Medicine, Chinese Academy of Medical Sciences (No. 2019RU013), College of Emergency and Trauma, Hainan Medical University, Haikou 571199, China;* ⓘ orcid.org/0000-0002-9050-2615

Bingya Wang — *College of Chemistry and Chemical Engineering, Xinyang Normal University, Xinyang 464000, China*

Yuxia Zou — *Key Laboratory of Emergency and Trauma, Ministry of Education, Key Laboratory of Hainan Trauma and Disaster Rescue, The First Affiliated Hospital of Hainan Medical University, Institute of Functional Materials and Molecular Imaging, Research Unit of Island Emergency Medicine, Chinese Academy of Medical Sciences (No. 2019RU013), College of Emergency and Trauma, Hainan Medical University, Haikou 571199, China*

Peiwen Fan — *College of Chemistry and Chemical Engineering, Xinyang Normal University, Xinyang 464000, China*

Xueping Chang — *College of Chemistry and Chemical Engineering, Xinyang Normal University, Xinyang 464000, China;* ⓘ orcid.org/0000-0002-8166-898X

Complete contact information is available at:
https://pubs.acs.org/10.1021/acssensors.0c00270

Author Contributions

§J.T.H., B.W., and Y.Z. contributed equally.

Notes

The authors declare no competing financial interest.

◼ REFERENCES

(1) Martel-Pelletier, J.; Barr, A. J.; Cicuttini, F. M.; Conaghan, P. G.; Cooper, C.; Goldring, M. B.; Goldring, S. R.; Jones, G.; Teichtahl, A. J.; Pelletier, J. P. Osteoarthritis. *Nat. Rev. Dis. Primers* **2016**, *2*, 16072.

(2) Loeser, R. F.; Collins, J. A.; Diekman, B. O. Ageing and the pathogenesis of osteoarthritis. *Nat. Rev. Rheumatol.* **2016**, *12*, 412−420.

(3) Zhang, L.; Hu, J.; Athanasiou, K. A. The role of tissue engineering in articular cartilage repair and regeneration. *Crit. Rev. Biomed. Eng.* **2009**, *37*, 1−57.

(4) Mobasheri, A.; Rayman, M. P.; Gualillo, O.; Sellam, J.; van der Kraan, P.; Fearon, U. The role of metabolism in the pathogenesis of osteoarthritis. *Nat. Rev. Rheumatol.* **2017**, *13*, 302−311.

(5) Guermazi, A.; Niu, J.; Hayashi, D.; Roemer, F. W.; Englund, M.; Neogi, T.; Aliabadi, P.; McLennan, C. E.; Felson, D. T. Prevalence of abnormalities in knees detected by MRI in adults without knee osteoarthritis: population based observational study (Framingham Osteoarthritis Study). *BMJ* **2012**, *345*, No. e5339.

(6) Scanzello, C. R. Role of low-grade inflammation in osteoarthritis. *Curr. Opin. Rheumatol.* **2017**, *29*, 79−85.

(7) Zhao, L.-R.; Xing, R.-L.; Wang, P.-M.; Zhang, N.-S.; Yin, S.-J.; Li, X.-C.; Zhang, L. NLRP1 and NLRP3 inflammasomes mediate LPS/ ATP-induced pyroptosis in knee osteoarthritis. *Mol. Med. Rep.* **2018**, *17*, 5463−5469.

(8) Steinbeck, M. J.; Nesti, L. J.; Sharkey, P. F.; Parvizi, J. Myeloperoxidase and chlorinated peptides in osteoarthritis: potential biomarkers of the disease. *J. Orthop. Res.* **2007**, *25*, 1128−1135.

(9) Flugge, L. A.; Miller-Deist, L. A.; Petillo, P. A. Towards a molecular understanding of arthritis. *Chem. Biol.* **1999**, *6*, R157−R166.

(10) Daumer, K. M.; Khan, A. U.; Steinbeck, M. J. Chlorination of pyridinium compounds possible role of hypochlorite, n-chloramines, and chlorine in the oxidation of pyridinoline cross-links of articular cartilage collagen type ii during acute inflammation. *J. Biol. Chem.* **2000**, *275*, 34681−34692.

(11) Lin, V. S.; Chen, W.; Xian, M.; Chang, C. J. Chemical probes for molecular imaging and detection of hydrogen sulfide and reactive sulfur species in biological systems. *Chem. Soc. Rev.* **2015**, *44*, 4596−4618.

(12) Hou, J.-T.; Ren, W. X.; Li, K.; Seo, J.; Sharma, A.; Yu, X.-Q.; Kim, J. S. Fluorescent bioimaging of pH: from design to applications. *Chem. Soc. Rev.* **2017**, *46*, 2076−2090.

(13) Gao, M.; Yu, F.; Lv, C.; Choo, J.; Chen, L. Fluorescent chemical probes for accurate tumor diagnosis and targeting therapy. *Chem. Soc. Rev.* **2017**, *46*, 2237−2271.

(14) Wu, D.; Sedgwick, A. C.; Gunnlaugsson, T.; Akkaya, E. U.; Yoon, J.; James, T. D. Fluorescent chemosensors: the past, present and future. *Chem. Soc. Rev.* **2017**, *46*, 7105−7123.

(15) Wu, X.; Shi, W.; Li, X.; Ma, H. Recognition moieties of small molecular fluorescent probes for bioimaging of enzymes. *Acc. Chem. Res.* **2019**, *52*, 1892−1904.

(16) Hou, J. T.; Ko, K. P.; Shi, H.; Ren, W. X.; Verwilst, P.; Koo, S.; Lee, J. Y.; Chi, S. G.; Kim, J. S. PLK1-targeted fluorescent tumor imaging with high signal-to-background ratio. *ACS Sens.* **2017**, *2*, 1512−1516.

(17) Zhang, R.; Song, B.; Yuan, J. Bioanalytical methods for hypochlorous acid detection: Recent advances and challenges. *TrAC, Trends Anal. Chem.* **2018**, *99*, 1−33.

(18) Ren, M.; Zhou, K.; He, L.; Lin, W. Mitochondria and lysosome-targetable fluorescent probes for HOCl: recent advances and perspectives. *J. Mater. Chem. B* **2018**, *6*, 1716−1733.

(19) Duan, C.; Won, M.; Verwilst, P.; Xu, J.; Kim, H. S.; Zeng, L.; Kim, J. S. In vivo imaging of endogenously produced hclo in zebrafish and mice using a bright, photostable ratiometric fluorescent probe. *Anal. Chem.* **2019**, *91*, 4172−4178.

(20) Li, G.; Lin, Q.; Sun, L.; Feng, C.; Zhang, P.; Yu, B.; Chen, Y.; Wen, Y.; Wang, H.; Ji, L.; Chao, H. A mitochondrial targeted two-photon iridium (III) phosphorescent probe for selective detection of hypochlorite in live cells and in vivo. *Biomaterials* **2015**, *53*, 285−295.

(21) Yuan, L.; Wang, L.; Agrawalla, B. K.; Park, S.-J.; Zhu, H.; Sivaraman, B.; Peng, J.; Xu, Q.-H.; Chang, Y.-T. Development of targetable two-photon fluorescent probes to image hypochlorous acid in mitochondria and lysosome in live cell and inflamed mouse model. *J. Am. Chem. Soc.* **2015**, *137*, 5930−5938.

(22) Hu, J. J.; Wong, N.-K.; Lu, M.-Y.; Chen, X.; Ye, S.; Zhao, A. Q.; Gao, P.; Kao, R. Y.-T.; Shen, J.; Yang, D. HKOCl-3: a fluorescent hypochlorous acid probe for live-cell and in vivo imaging and quantitative application in flow cytometry and a 96-well microplate assay. *Chem. Sci.* **2016**, *7*, 2094−2099.

(23) Chen, X.; Lee, K.-A.; Ren, X.; Ryu, J.-C.; Kim, G.; Ryu, J.-H.; Lee, W.-J.; Yoon, J. Synthesis of a highly HOCl-selective fluorescent probe and its use for imaging HOCl in cells and organisms. *Nat. Protoc.* **2016**, *11*, 1219−1228.

(24) Zhang, B.; Yang, X.; Zhang, R.; Liu, Y.; Ren, X.; Xian, M.; Ye, Y.; Zhao, Y. Lysosomal-targeted two-photon fluorescent probe to sense hypochlorous acid in live cells. *Anal. Chem.* **2017**, *89*, 10384−10390.

(25) Mao, Z.; Ye, M.; Hu, W.; Ye, X.; Wang, Y.; Zhang, H.; Li, C.; Liu, Z. Design of a ratiometric two-photon probe for imaging of hypochlorous acid (HClO) in wounded tissues. *Chem. Sci.* **2018**, *9*, 6035−6040.

(26) Pak, Y. L.; Park, S. J.; Wu, D.; Cheon, B.; Kim, H. M.; Bouffard, J.; Yoon, J. N-Heterocyclic carbene boranes as reactive oxygen species-responsive materials: application to the two-photon imaging of hypochlorous acid in living cells and tissues. *Angew. Chem., Int. Ed.* **2018**, *57*, 1567−1571.

(27) Shi, D.; Chen, S.; Dong, B.; Zhang, Y.; Sheng, C.; James, T. D.; Guo, Y. Evaluation of HOCl-generating anticancer agents by an ultrasensitive dual-mode fluorescent probe. *Chem. Sci.* **2019**, *10*, 3715−3722.

(28) Wang, J.; Cheng, D.; Zhu, L.; Wang, P.; Liu, H.-W.; Chen, M.; Yuan, L.; Zhang, X.-B. Engineering dithiobenzoic acid lactone-decorated Si-rhodamine as a highly selective near-infrared HOCl fluorescent probe for imaging drug-induced acute nephrotoxicity. *Chem. Commun.* **2019**, *55*, 10916−10919.

(29) Hou, J.-T.; Kim, H. S.; Duan, C.; Ji, M. S.; Wang, S.; Zeng, L.; Ren, W. X.; Kim, J. S. A ratiometric fluorescent probe for detecting hypochlorite in the endoplasmic reticulum. *Chem. Commun.* **2019**, *55*, 2533−2536.

(30) Wei, P.; Liu, L.; Wen, Y.; Zhao, G.; Xue, F.; Yuan, W.; Li, R.; Zhong, Y.; Zhang, M.; Yi, T. Release of amino- or carboxy-containing compounds triggered by HOCL: application for imaging and drug design. *Angew. Chem., Int. Ed.* **2019**, *58*, 4547−4551.

(31) Hou, J.-T.; Yu, K.-K.; Sunwoo, K.; Kim, W. Y.; Koo, S.; Wang, J.; Ren, W. X.; Wang, S.; Yu, X.-Q.; Kim, J. S. Fluorescent imaging of reactive oxygen and nitrogen species associated with pathophysiological processes. *Chem* **2020**, *6*, 832−866.

(32) Feng, H.; Zhang, Z.; Meng, Q.; Jia, H.; Wang, Y.; Zhang, R. Rapid response fluorescence probe enabled in vivo diagnosis and assessing treatment response of hypochlorous acid-mediated rheumatoid arthritis. *Adv. Sci.* **2018**, *5*, 1800397.

(33) Wei, P.; Yuan, W.; Xue, F.; Zhou, W.; Li, R.; Zhang, D.; Yi, T. Deformylation reaction-based probe for in vivo imaging of HOCl. *Chem. Sci.* **2018**, *9*, 495−501.

(34) Kang, J.; Huo, F.; Zhang, Y.; Chao, J.; Strongin, R. M.; Yin, C. Detecting intracellular ClO- with ratiometric fluorescent signal and its application7 in vivo. *Sens. Actuators B* **2018**, *273*, 1532−1538.

(35) Cao, C.; Zhou, X.; Xue, M.; Han, C.; Feng, W.; Li, F. Dual near-infrared-emissive luminescent nanoprobes for ratiometric luminescent monitoring of ClO⁻ in living organisms. *ACS Appl. Mater. Interfaces* **2019**, *11*, 15298−15305.

(36) Wang, S.; Zhu, B.; Wang, B.; Fan, P.; Jiu, Y.; Zhang, M.; Jiang, L.; Hou, J.-T. A highly selective phenothiazine-based fluorescent chemosensor for phosgene. *Dyes Pigm.* **2020**, *173*, 107933.

(37) Xiao, H.; Xin, K.; Dou, H.; Yin, G.; Quan, Y.; Wang, R. A fast-responsive mitochondria-targeted fluorescent probe detecting endogenous hypochlorite in living RAW 264.7 cells and nude mouse. *Chem. Commun.* **2015**, *51*, 1442−1445.

(38) Yin, C.; Zhu, H.; Xie, C.; Zhang, L.; Chen, P.; Fan, Q.; Huang, W.; Pu, K. Organic nanoprobe cocktails for multilocal and multicolor fluorescence imaging of reactive oxygen species. *Adv. Funct. Mater.* **2017**, *27*, 1700493.

(39) Jiao, X.; Huang, K.; He, S.; Liu, C.; Zhao, L.; Zeng, X. A mitochondria-targeted near-infrared fluorescent probe with a large Stokes shift for real-time detection of hypochlorous acid. *Org. Biomol. Chem.* **2019**, *17*, 108−114.

(40) Liu, F.; Wu, T.; Cao, J.; Zhang, H.; Hu, M.; Sun, S.; Song, F.; Fan, J.; Wang, J.; Peng, X. A novel fluorescent sensor for detection of highly reactive oxygen species, and for imaging such endogenous hROS in the mitochondria of living cells. *Analyst* **2013**, *138*, 775−778.

(41) Cao, D.; Liu, Z.; Verwilst, P.; Koo, S.; Jangjili, P.; Kim, J. S.; Lin, W. Coumarin-based small-molecule fluorescent chemosensors. *Chem. Rev* **2019**, *119*, 10403−10519.

(42) Becke, A. D. A new mixing of hartree-fock and local density-functional theories. *J. Chem. Phys.* **1993**, *98*, 1372−1377.

(43) Francl, M. M.; Pietro, W. J.; Hehre, W. J.; Binkley, J. S.; Gordon, M. S.; DeFrees, D. J.; Pople, J. A. Self-consistent molecular orbital methods. xxiii. a polarization-type basis set for second-row elements. *J. Chem. Phys.* **1982**, *77*, 3654−3665.

(44) Frisch, M. J.; Trucks, G. W.; Schlegel, H. B.; Scuseria, G. E.; Robb, M. A.; Cheesem, J. R.; Scalmani, G.; Barone, V.; Mennucci, B.; Petersson, G. A. *Gaussian 09, rev. A.02*; Gaussian, Inc.: Wallingford, CT, 2009.

(45) Schmidt, R. L.; Simonović, M. Synthesis and decoding of selenocysteine and human health. *Croat. Med. J.* **2012**, *53*, 535−550.

(46) Li, F.; Lutz, P. B.; Pepelyayeva, Y.; Arnér, E. S. J.; Bayse, C. A.; Rozovsky, S. Redox active motifs in selenoproteins. *Proc. Natl. Acad. Sci.* **2014**, *111*, 6976−6981.

(47) Han, X.; Wang, R.; Song, X.; Yu, F.; Chen, L. Evaluation selenocysteine protective effect in carbon disulfide induced hepatitis with a mitochondrial targeting ratiometric near-infrared fluorescent probe. *Anal. Chem.* **2018**, *90*, 8108−8115.

(48) Kalunian, K. C. Current advances in therapies for osteoarthritis. *Curr. Opin. Rheumatol.* **2016**, *28*, 246−250.

(49) Han, X.; Song, X.; Yu, F.; Chen, L. A ratiometric near-infrared fluorescent probe for quantification and evaluation of selenocysteine-protective effects in acute inflammation. *Adv. Funct. Mater.* **2017**, *27*, 1700769.

(50) Huang, Z. Y.; Stabler, T.; Pei, F. X.; Kraus, V. B. Both systemic and local lipopolysaccharide (LPS) burden are associated with knee OA severity and inflammation. *Osteoarthr. Cartilage* **2016**, *24*, 1769−1775.